Molecular Biology of the Cell
Vol. 20, 4183–4193, October 1, 2009

# Udu Deficiency Activates DNA Damage Checkpoint

**Chiaw-Hwee Lim,* Shang-Wei Chong,* and Yun-Jin Jiang*†‡**

*Laboratory of Developmental Signalling and Patterning, Genes and Development Division, Institute of Molecular and Cell Biology, Agency for Science, Technology and Research, Singapore 138673; †Department of Biochemistry, National University of Singapore, Singapore 117597; and ‡School of Biological Sciences, Nanyang Technological University, Singapore 637551

Submitted February 5, 2009; Revised July 9, 2009; Accepted July 27, 2009
Monitoring Editor: Orna Cohen-Fix

**Udu has been shown to play an essential role during blood cell development; however, its roles in other cellular processes remain largely unexplored. In addition, *u*gly *du*ckling (*udu*) mutants exhibited somite and myotome boundary defects. Our fluorescence-activated cell sorting analysis also showed that the loss of *udu* function resulted in defective cell cycle progression and comet assay indicated the presence of increased DNA damage in $udu^{tu24}$ mutants. We further showed that the extensive p53-dependent apoptosis in $udu^{tu24}$ mutants is a consequence of activation in the Atm–Chk2 pathway. Udu seems not to be required for DNA repair, because both wild-type and *udu* embryos similarly respond to and recover from UV treatment. Yeast two-hybrid and coimmunoprecipitation data demonstrated that PAH-L repeats and SANT-L domain of Udu interacts with MCM3 and MCM4. Furthermore, Udu is colocalized with 5-bromo-2′-deoxyuridine and heterochromatin during DNA replication, suggesting a role in maintaining genome integrity.**

## INTRODUCTION

*u*gly *du*ckling ($udu^{tu24}$) mutant was first isolated from the 1996 Tübingen screen and has been shown to exhibit a short body-axis with massive cell death (Hammerschmidt *et al*., 1996). Another *udu* allele, $udu^{sq1}$, was isolated in a genetic screen aiming at mutants with defects in hematopoiesis (Liu *et al*., 2007). Positional cloning revealed that Udu protein encodes a novel nuclear factor consisting of three *c*onserved *r*egions (CR-1, CR-2, and CR-3) that do not share similarity with any known domains, two *p*aired *a*mphipathic α-*h*elix *l*ike (PAH-L) repeats, and one putative *S*W13, *A*DA2, *N*-Cor and *T*FIIIB *l*ike (SANT-L) domain. The C-terminal PAH-L and SANT-L domains have been shown to be essential in primitive erythroid cell development (Liu *et al*., 2007). The PAH domain, first identified in yeast SIN3 (Wang *et al*., 1990), has been demonstrated to mediate protein–protein interactions (Spronk *et al*., 2000). SIN3 has no intrinsic DNA binding ability and has to be targeted to gene promoters by interacting with DNA binding proteins, thereafter positively and negatively regulating genes involved in diverse cellular functions (Silverstein and Ekwall, 2005). The SANT domain is a highly conserved motif with similarity to Myb DNA binding domain (Aasland *et al*., 1996), which has been shown to be critical in regulating chromatin accessibility (Boyer *et al*., 2002, 2004).

The DNA damage response pathway is a cellular surveillance system that senses the presence of damaged DNA and elicits checkpoint activation and subsequent lesion repair in preventing amplification or loss of genes or chromosomes (Zhou and Elledge, 2000). The critical components of DNA damage checkpoint are two phosphatidyl inositol 3-kinase-like kinase family proteins: *A*taxia *t*elangiectasia *m*utated (ATM) and *AT*M- and *R*ad3-related (ATR) (Abraham, 2003; Shiloh, 2003). ATR functions as a sensor and transducer in response to UV light and presumably to genotoxic agents that give rise to stalled replication forks, and subsequently activates *Ch*eckpoint *k*inase (Chk) 1 (Melo *et al*., 2001), whereas ATM is a central signaling protein that functions in response to DNA *d*ouble-stranded *b*reaks (DSBs), leading to activation of Chk2 (Shiloh, 2003), which ultimately activates the tumor suppressor p53 (Helton and Chen, 2007). On p53 phosphorylation through ATM, its interaction with Mdm2 is inhibited, resulting in p53 stabilization (Shieh *et al*., 1997). p53 accumulates in the nucleus and regulates transcription of genes involved in DNA damage response by eliciting cell cycle arrest and/or apoptosis and thereby constraining tumor progression (Lane, 1992; Ljungman, 2000).

Most of the genes targeted by p53 are associated with the regulation of cell cycle arrest, apoptosis and/or DNA repair processes, which function to prevent proliferation of damaged cells. The central components of the cell cycle system are cyclins and *c*yclin-*d*ependent *k*inases (CDKs). A major player in the p53-mediated G1 arrest is $p21^{WAF/CIP1}$ that inhibits cyclin E-CDK2. Thus, an accumulation of $p21^{WAF/CIP1}$ prevents G1-to-S transition and aberrant replication of damaged DNA (Waldman *et al*., 1995). p53 also plays a critical role in G2 arrest that allows cells to avoid segregation of defective chromosomes through the regulation of many target genes during G2/M arrest (Bunz *et al*., 1998). For example, *g*rowth-*a*rrest and *D*NA *d*amage-inducible 45 (GADD45) proteins can associate with $p21^{WAF/CIP1}$, which inhibits G1-

This article was published online ahead of print in *MBC in Press* (http://www.molbiolcell.org/cgi/doi/10.1091/mbc.E09–02–0109) on August 5, 2009.

Address correspondence to: Yun-Jin Jiang (yjjiang@imcb.a-star.edu.sg).

Abbreviations used: ATM, Ataxia telangiectasia mutated; ATR, ATM- and Rad3-related; Chk, checkpoint kinase; GADD45, growth-arrest and DNA damage-inducible 45; hpf, hours postfertilization; MCM, minichromosome maintenance; MO, morpholino; PAH-L, paired amphipathic α-helix like; pH3, phosphorylated histone H3; SANT-L, SW13, ADA2, N-Cor and TFIIIB like; ss, somite stage; *udu*, *ugly duckling*.

to-S phase transition and also promotes dissociation of the *c*ell *d*ivision *c*ontrol (Cdc)2/cyclin B1 complex, inducing a G2/M arrest (Fornace *et al*., 1992; Vairapandi *et al*., 1996; Wang *et al*., 1999; Mak and Kultz, 2004).

*M*inichromosome *m*aintenance (MCM) proteins are conserved in eukaryotes and have essential roles in initiation and elongation during DNA replication (Tye, 1999; Labib *et al*., 2000; Forsburg, 2004; Pacek and Walter, 2004; Shechter *et al*., 2004). MCM4, -6, and -7 have been shown to unwind DNA helices in a ATP-dependent manner, whereas the heterohexameric MCM2-7 does not, suggesting that MCM4, -6, and -7 may function as the catalytic core and the replicative helicase during DNA replication (Fujita *et al*., 1997; Kubota *et al*., 1997; Labib *et al*., 2000). Association of the MCM complex with the chromatin is cell cycle regulated: MCM2-7 binds to chromatin only during the G1/S phase and dissociates from as replication proceeds (Kearsey and Labib, 1998). Moreover, loss of MCM function has been demonstrated to cause DNA damage and genome instability (Bailis and Forsburg, 2004).

Here, we investigated what causes *p53* up-regulation and developmental defects that are associated with the loss of *udu* function. We demonstrated that the DNA damage response pathway, containing Atm-Chk2-p53, is activated in $udu^{tu24}$ mutants. The PAH-L and SANT-L domains of Udu were found to be involved in protein–protein interactions with MCM3 and MCM4. Our data indicate that Udu deficiency during zebrafish development causes genomic instability, leading to an activation of the DNA damage checkpoint, which activates p53 and subsequently results in the cell cycle arrest and apoptosis. To our knowledge, this work provides the first biochemical link between PAH-L and SANT-L domains and MCM proteins and a possible functional link between Udu and DNA replication.

## MATERIALS AND METHODS

### *Embryos*

Wild-type and $udu^{tu24}$ (Hammerschmidt *et al*., 1996) embryos were staged as described previously (Kimmel *et al*., 1995). Dechorinated embryos were placed ~65 cm from a UV bulb (SYLVANIA Germicidal G30T8/30 W), irradiated for 15 min, and subsequently rinsed several times in E3 medium and then incubated at 28.5°C for 1 h before any subsequent experiments were carried out. Embryos were soaked in KU55933 (ATM kinase inhibitor) at 15 $\mu$M and CGK733 (ATM/ATR kinase inhibitor) at 200 $\mu$M for 20 h. All experiments on zebrafish embryos were approved by the Biological Research Centre, Agency for Science, Technology and Research (Singapore).

### *Injection Experiments*

Morpholinos (MOs) (Gene Tools, Philomath, OR) were dissolved in 1× Danieau buffer and stored at −20°C. We injected 1.77 pmol of *p53*-MO (5′-GCGCCATTGCTTTGCAAGAATTG-3′; Langheinrich *et al*., 2002), 0.78 pmol of *atm*-MO (5′-GAAAACGGCACCACCTGGTAAA-3′; Yamaguchi *et al*., 2008), and 2.08 pmol of *chk2*-MO (5′-CAGACATGATGCTTTTATTCTGGAC-3′; Yamaguchi *et al*., 2008) into the yolks of one- to four-cell stage embryos.

### *Genotyping of $udu^{tu24}$ Embryos*

Homozygous $udu^{tu24}$ embryos injected with *p53*-MO were selected based on somite phenotype described and shown in Supplemental Figure S1E. Homozygous $udu^{tu24}$ embryos injected with *chk2*-MO have tail-tips that were not round-shaped but tapered (see Figure 4N). Selected *p53*-MO– and *chk2*-MO–injected $udu^{tu24}$ embryos were subjected to sequencing experiments to confirm their genotype. Homozygous $udu^{tu24}$ embryos were identified via polymerase chain reaction (PCR) amplification of genomic DNA by using forward (5′-TTGGCTCAACCAGTGTAAA-3′) and reverse (5′-TGTGAATGTTACCTAATAGC-3′) primers. Sequencing of these PCR fragments revealed a T-to-A transition in exon 12 of the mutant embryos, shown in Supplemental Figure S1F.

### *RNA Isolation and Quantitative Real-Time PCR*

RNA was isolated from wild-type and $udu^{tu24}$ embryos at the respective stage by using TRIzol reagent (Invitrogen, Carlsbad, CA). Total RNA was reversely transcribed using Superscript II reverse transcriptase (Invitrogen) and cDNA was amplified with the respective primers designed using Primer Express software, version 3.0 (Applied Biosystems, Foster City, CA). The SYBR Green-based quantitative real-time PCR was carried out on an ABI 7300 real-time PCR system. Reactions were performed using SYBR Green PCR master mix (Applied Biosystems) for one cycle of 95°C for 10 min, followed by 44 cycles of 95°C for 15 s and 60°C for 1 min. *elf1a* was used as an endogenous control. Relative quantification was performed using Prism Sequence Detection software (Applied Biosystems). Gene accession numbers and primer sequences used for the quantitative real-time PCR are presented in Supplemental Table 1.

### *Plasmids*

The construct of PAH-L and SANT-L domains was made by subcloning the PCR-amplified fragments into pcDNA3.1(+) vector. We used forward (5′-CCTCCACAGATCAGCGAGGGTACCATGGATTACAAGGACGACGATGACAAGGGAGGCCGT-3′) and reverse (5′-CTGCTCTGCAGCCTCGAGCTCTGAACTGGCCTG-3′) primers to amplify the PAH-L and SANT-L domains. HP1$\beta$, MCM3, and MCM4 PCR-amplified fragments were made by subcloning the PCR-amplified fragments into pCS2+MT vector. We used forward (5′-AAAAGATCTGGGAATTCCATGGCTGCTGAAGTTGTG-3′) and reverse (5′-ACTGATATTGTCCCGCTCGAGCGGTTAAATCAGGAA-3′) to amplify *mcm3*; forward (5′-CGCACGTTTTGGAATTCCATGTCTTCACCATCA-3′) and reverse (5′-TCCTGGGATCAGTTGCTCTAGAGCTCAGGGCTTCTCGAT-3′) to amplify *mcm4*; forward (5′-AGAGCCTCGGGATCCATGAGCCAACCTACA-3′) and reverse (5′-TGACTTGCCATCGATCTAGTTCTTGTCATC-3′) to amplify *hp1*$\beta$. Total RNA was reversely transcribed using SuperScript II reverse transcriptase (Invitrogen), and all PCR amplification experiments were done using Expand High Fidelity PCR System (Roche, Basel, Switzerland). All PCR amplified sequences were verified using SeqMan II, expert sequence analysis (DNASTAR, Madison, WI).

### *Whole-Mount mRNA In Situ Hybridization (WISH) and Immunohistochemical Staining*

Digoxigenin-labeled antisense RNA probes were generated with a Stratagene RNA transcription kit. Single WISH was done as described previously (Qiu *et al*., 2004). For immunohistochemical staining, embryos were anesthetized, dechorinated and fixed in 4% paraformaldehyde (PFA)/phosphate-buffered saline (PBS) at 4°C, unless otherwise stated. The following antibodies were used: mouse anti-$\beta$-catenin (Abcam, Cambridge, United Kingdom) and polyclonal rabbit anti-phosphorylated histone H3 (pH3) (Cell Signaling Technology, Danvers, MA). The appropriate AlexaFluor-conjugated secondary antibodies (Invitrogen) were used for signal detection. Embryos were counterstained with 4,6-diamidino-2-phenylindole (DAPI) (Sigma-Aldrich, St. Louis, MO) to visualize cell nuclei. Embryos labeled with pH3 antibody and DAPI were scanned using confocal microscope, and the numbers of dividing cells and total cells were counted. Immunohistochemical staining of $\gamma$-H2AX antibody (Novus Biologicals, Littleton, CO) was carried out on embryos fixed in acetone: methanol (50:50).

### *5-Bromo-2′-deoxyuridine (BrdU) Incorporation*

For labeling of S phase cells, BrdU was incorporated by incubating dechorinated live zebrafish embryos in BrdU solution (10 mM BrdU; 15% dimethyl sulfoxide [DMSO] in E3 medium) for 20 min on ice, followed by washes in E3 medium and further incubation for 1 h at 28.5°C. Embryos were then fixed in 4% PFA/PBS overnight at 4°C. After several washes in 0.1% Tween in PBS (PBST), embryos were incubated in 100% methanol overnight at −20°C. Embryos were permeabilized with proteinase K, refixed in 4% PFA for 20 min, and then rinsed in PBST and 2 N HCl, and followed by incubation in 2 N HCl for 1 h. Subsequently, embryos were blocked for 1 h in blocking solution and incubated with primary anti-BrdU antibody (Sigma-Aldrich) and secondary AlexaFluor488-conjugated anti-mouse antibody (Invitrogen).

### *Fluorescence-Activated Cell Sorting (FACS) and Cell Cycle Analysis*

Whole embryos or tail region posterior to yolk extension at 22 h postfertilization (hpf) were used. Single-cell suspension was obtained as described previously (Ryu *et al*., 2005). Cells were resuspended in 4 mM citrate buffer, pH 6.5, containing 0.1 mg/ml propidium iodide, 200 $\mu$g/ml RNase, and 0.1% Triton X-100. Cell cycle progression was analyzed using FACScan machine (BD Biosciences, San Jose, CA).

### *Detection of Apoptotic Cells in Whole-Mount and Cryostat Section*

The fragmented DNA of apoptotic cells was identified by the *t*erminal deoxynucleotidyl transferase-mediated biotinylated d*U*TP *n*ick *e*nd *l*abeling (TUNEL) method, by using the AP, In Situ Cell Death Detection kit (Roche) and the DeadEnd TUNEL system (Promega, Madison, WI), according to the manufacturer's instructions. For cryostat sections, embryos were embedded in OCT medium as described in the zebrafish book (http://www.zfin.org).

### *Comet Assays*

Neutral comet assay was performed using the CometAssay kit (4250-040-K; Trevigen, Gaithersburg, MD) according to the manufacturer's instruction. DNA was stained with SYBR Green as provided (Trevigen). Comet images were taken by fluorescence microscopy.

### *Nuclear Protein Extraction*

Yolks were removed from zebrafish embryos (22 hpf) by using ice-cold PBS with protease inhibitor cocktail (Roche) by pipetting with a 200-$\mu$l tip. Nuclear protein was obtained from the yolk-extirpated embryos according to the protocol described in Davuluri *et al.* (2008). The extracted proteins were electrophoresed on an SDS-polyacrylamide gel followed by Western blotting with rabbit anti-Chk2 (Cell Signaling Technology) and rabbit anti-phospho-Chk2 (Ser33) (Cell Signaling Technology). We used 5% bovine serum albumin for blocking. $\beta$-Tubulin (Abcam) was used as a loading control.

### *Cell Culture, Transfection, Immunoprecipitation, and Synchronization*

COS7 cells were cultured in DMEM supplemented with 10% (vol/vol) fetal bovine serum and 1% penicillin-streptomycin. Cells were transiently transfected using Lipofectamine LTX transfection reagent (Invitrogen). In immunoprecipitation assay, cells were harvested 24 h after transfection in IONIC buffer (50 mM Tris, pH 8.0, 150 mM NaCl, 0.5% NP-40, 0.5% deoxycholic acid, and 0.05% SDS, containing protease inhibitor cocktail [Roche]). Cell lysate from 100-mm dish was clarified by centrifugation and incubated with anti-FLAG M2 affinity gel (Sigma-Aldrich) for 4 h at 4°C. The eluted proteins were electrophoresed on an SDS-polyacrylamide gel followed by Western blotting with rabbit anti-Myc (Santa Cruz Biotechnology, Santa Cruz, CA) and rabbit anti-FLAG antibodies (Santa Cruz Biotechnology). For cell synchronization, COS7 cells were incubated in 1 $\mu$g/ml aphidicolin (Calbiochem, San Diego, CA) for 20 h and then released into aphidicolin-free medium. Cells were confirmed in G1/S border by FACS analysis. Synchronized cells were then incubated in 10 $\mu$M BrdU for 10 min at 37°C.

### *Immunofluorescence*

COS7 cells were grown on coverslips under the conditions as described in Cell Culture, Transfection, Immunoprecipitation, and Synchronization. After 24-h transfection, cells were fixed in 4% PFA/PBS for 10 min at room temperature. Fixed cells were permeabilized in 0.1% Triton X-100 in PBS for 10 min and then blocked in blocking solution (10% goat serum in PBS) for 1 h. The cells were then sequentially treated with primary and secondary antibodies diluted in blocking solution for 1 h each at room temperature. The primary antibodies used were rabbit anti-FLAG (Santa Cruz Biotechnology), mouse anti-BrdU (Sigma-Aldrich), and mouse anti-Myc (Santa Cruz Biotechnology) and polyclonal anti-Udu (Liu *et al.*, 2007). The secondary antibodies used were Alexa488 goat anti-rabbit and Alexa568 goat anti-mouse antibodies (Invitrogen).

### *Microscopy*

Embryos were observed on an Axioskop microscope (Carl Zeiss, Jena, Germany) equipped with a camera (Nikon, Tokyo, Japan) for digital image capture. Confocal images of TUNEL and BrdU assays were taken on an inverted 510 LSM laser scanning confocal microscope (Carl Zeiss), and images were processed using LSM image browser (Carl Zeiss). pH3 and $\gamma$-H2AX immunohistochemical staining and immunofluorescence assays were taken on a FluoView upright confocal microscope (Olympus, Tokyo, Japan) equipped with FV10-ASW 1.6 viewer. All images were assembled using Photoshop (Adobe Systems, Mountain View, CA).

## RESULTS

### *udu$^{tu24}$ Mutants Exhibit Defects in Somites and Myotome Boundaries*

The earliest morphological *udu$^{tu24}$* phenotype could be observed at 15.5 hpf (13 somite stage [ss]) to 16.5 hpf (15 ss): the regular somite morphology was lost and tail failed to extend properly (data not shown). At 20 hpf, the short body-axis was more evident; the boundaries of the posterior somites were not chevron-shaped and lacked clear boundaries. Overall, *udu$^{tu24}$* mutants displayed a retarded growth, with reduced number of formed somites (Figure 1, A and B). At day 2, *udu$^{tu24}$* mutants showed a significant reduction in body length, yolk sac extension as well as smaller head and eyes (Figure 1, C and D). Maternal *udu* mRNA transcript was detected from one-cell stage and diminished during gastrula; zygotic transcript reappeared in a ubiquitous manner and was enriched in specific tissues later (Liu *et al.*, 2007). The maternal *udu* contribution may attribute to the late onset of observable phenotypes in *udu$^{tu24}$* mutants.

Next, we investigated the somite defects in *udu$^{tu24}$* mutants with various somite markers. At 14 hpf (10 ss), *myoD* was expressed in adaxial cells and in the posterior half of the formed somites of wild-type embryos (Weinberg *et al.*, 1996); however, *myoD*-expressing cells were only found in the adaxial cells of *udu$^{tu24}$* mutants, an indication of developmental retardation (Figure 1, E and F). In 18 hpf (18 ss) wild-type embryos, *papc* is expressed in the anterior parts of nascent somites, segmental stripes in the anterior *p*resomitic *m*esoderm (PSM) and at lower level in the posterior PSM (Yamamoto *et al.*, 1998). The absence of *papc* expression in the anterior parts of nascent somites in *udu$^{tu24}$* mutants indicated the defects in anterior somite specification (Figure 1, G and H). Normaski images have demonstrated that the somite boundaries of *udu$^{tu24}$* embryos were not formed properly (Figure 1, I and J), which were further highlighted by membrane-localized $\beta$-catenin antibody (Supplemental Figures S2, A and B).

To examine whether the oscillator mechanism regulating zebrafish somite segmentation is affected, we analyzed *deltaC* expression, which is a readout of the cycling segmentation clock and prefigures the reiterated somites 60–90 min, time for generating two to three somites, before they physically form a boundary (Jiang *et al.*, 2000). In the mutants, cycling *deltaC* expression in the PSM was maintained at 12 and 15 ss, suggesting that the clock functions normally, at least at the onset of *udu* somite phenotype and is not responsible for the somite boundary defects (Supplemental Figure S3).

### *Dramatically Increased Apoptotic Cells Are Found in Specific Tissues of udu$^{tu24}$ Mutants*

Apoptotic cells have been found in *udu* mutants previously (Hammerschmidt *et al.*, 1996; Liu *et al.*, 2007). We further analyzed the developing embryos for TUNEL-positive cells, to investigate whether the severe morphological abnormality of *udu$^{tu24}$* mutants results from a spatial activation of the apoptotic pathway. The *udu$^{tu24}$* embryos had an extensive amount of TUNEL-positive cells in head, neural tube, and tail compared with wild-type embryos at 22 hpf (Figure 1, K and L). Examination of the TUNEL staining by sectioning revealed massive apoptotic cells in the midbrain–hindbrain region, the lens, and retina of *udu$^{tu24}$* mutants, whereas the otic placode remained unaffected (Figure 1, M–P). The mutant tail region was particularly concentrated with apoptotic cells, corresponding to the observed somite defects and short body length (Figure 1, Q and R). This analysis demonstrated that the increased activation of cellular apoptotic pathway correlates with regions of developmental abnormalities found in *udu$^{tu24}$* mutants.

### *Elevated Level of p53 Causes Apoptosis in udu$^{tu24}$ Embryos*

To examine whether the p53 pathway was activated in the apoptotic *udu$^{tu24}$* mutants, we examined *p53* transcript levels. Up-regulation of *p53* mRNA was obvious in the developing brain, pronephron, posterior trunk, and tail bud regions of *udu$^{tu24}$* embryos (Figure 2, A and B), which was correlated with the massive amount of TUNEL-positive cells found in corresponding regions (Figure 1, M–R). Next, *p53*-morpholino (MO) (Langheinrich *et al.*, 2002) injection was performed to examine whether elevated level of *p53* in *udu$^{tu24}$* mutants causes apoptosis. The knockdown of *p53* could significantly reduce the amount of TUNEL-positive cells and rescue somite defects in 65.9% (n = 29/44) of the

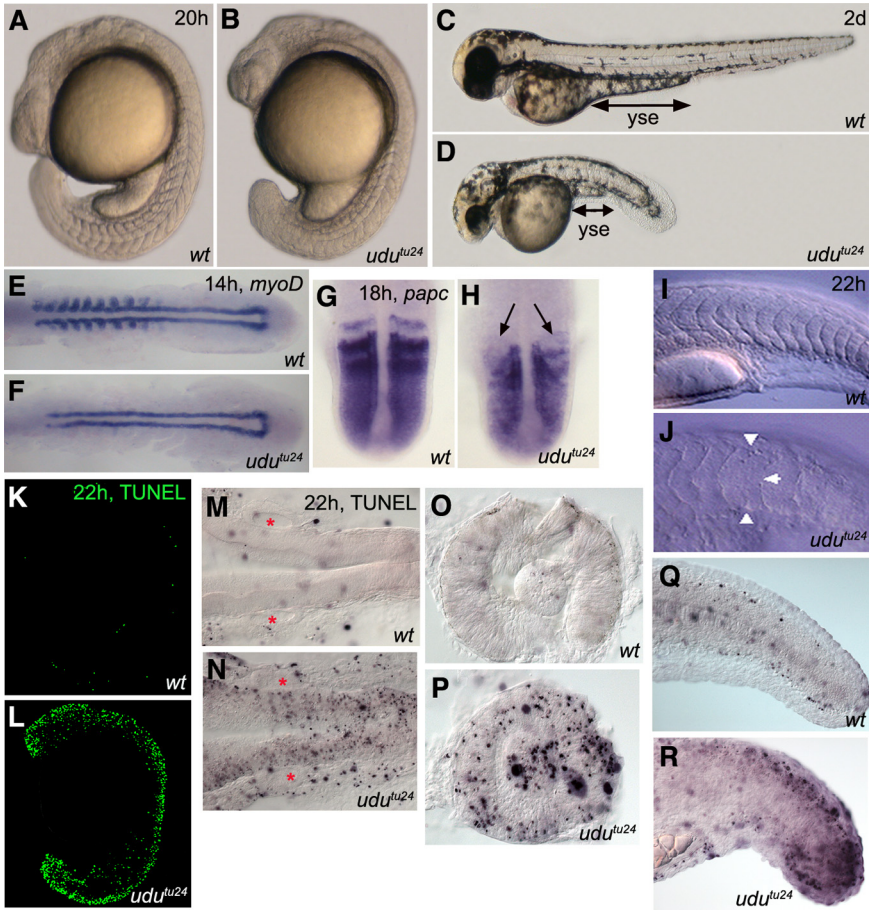


**Figure 1.** Developmental and apoptotic defects of *udu*$^{tu24}$ mutants. Morphology of wild-type and *udu*$^{tu24}$ mutants at 20 hpf (A and B) and 2 dpf (C and D). (E and F) WISH for *myoD* at 14 hpf. *myoD* is only expressed in the adaxial cells and is not detected in the posterior half of formed somites in *udu*$^{tu24}$ embryos. (G and H) WISH for *papc* at 18 hpf in dorsal view, with anterior upward. *papc* is not expressed in the nascent somites of *udu*$^{tu24}$ embryos; indicated by arrows. (I and J) Normaski images of wild-type and *udu*$^{tu24}$ embryos' somites (approximately the 12th to 24th somite region). Somites of wild-type embryos were chevron-shaped with clear boundaries; however, mutant somites were U-shaped and their boundaries were less distinct, indicated by arrowheads. All embryos are represented in lateral view with anterior to the left and dorsal upwards, unless otherwise stated. wt, wild type; yse, yolk sac extension. (K and L) TUNEL assay of whole-mount wild-type and *udu*$^{tu24}$ embryos. Massive amount of apoptotic cells are found throughout *udu*$^{tu24}$ embryos at 22 hpf. (M–R) Examination of sections of TUNEL staining in lateral view and anterior to the left, unless otherwise stated. Midbrain-hindbrain region, dorsal view (M and N), lens and retina (O and P), and tail region (Q and R) of *udu*$^{tu24}$ mutants consisted of many apoptotic cells compared with wild-type embryos. Areas marked by red asterisks denote the otic placode; eyes are removed and mounted in lateral view.

injected mutants (Figure 2, C–E, compared with Figure 1L). High-resolution images of somite structures are shown in Supplemental Figure S1. Consistently, *p53* MO-injected *udu*$^{tu24}$ mutants displayed a normal expression pattern of *myoD* and *titin* (Figure 2, F–I). Further evidence for the rescue of somite boundaries by *p53*-MO was presented as high-resolution confocal images of embryos labeled with β-catenin antibody (Supplemental Figure S2, C and D). Thus, inhibition of *p53* translation can suppress apoptosis and rescue developmental defects in *udu*$^{tu24}$ mutants.

To investigate whether genes involved in the *p53* pathway were up- or down-regulated in *udu*$^{tu24}$ embryos, real-time PCR was performed to determine the expression levels of *p53*, *mdm2*, *cyclin D1*, *p21*$^{WAF/CIP1}$, *caspase 8*, and *bax* and genes of the *gadd45* family. *p53* mRNA was obviously up-regulated in the mutants (Figure 2J), which corresponded to elevated level of *p53* shown previously with WISH. The level of *cyclin D1* was almost unaltered in *udu*$^{tu24}$ embryos, whereas downstream targets of the p53 pathway, including *mdm2*, *p21*$^{WAF/CIP1}$, *caspase 8*, and particularly *gadd45αl*, were up-regulated. Similarly, WISH confirmed that *gadd45αl* was indeed up-regulated in the trunk and tail regions of *udu*$^{tu24}$ embryos (data not shown). These data suggest that the apoptotic *udu*$^{tu24}$ phenotype is attributed to the activation of *p53* and its downstream target genes.

### *Loss of udu Function Results in Cell Cycle Defects*

With the up-regulation of *p53* and its response genes that are known to be involved in cell cycle and apoptosis, we performed FACS analysis of dissociated cells from whole body and tail region posterior to yolk extension of wild-type and *udu*$^{tu24}$ embryos stained with propidium-iodide (PI) to examine cell cycle progression. At 22 hpf, *udu*$^{tu24}$ mutants had a lower fraction of cells in the G1 and S phases and an accumulation of cells in the G2/M phase (Figure 3, A–F). To further verify the reduction of cell number in the S phase, incorporation of BrdU was carried out. The number of BrdU-positive cells was indeed much more reduced in *udu*$^{tu24}$ tail region posterior to yolk extension (Figure 3, G and H). Anti-pH3 antibody was used to label proliferating cells in the mitotic phase of 22 hpf embryos. Quantification of pH3-positive cells showed that the ratio of pH3-positive cells to the total number of cells at 22 hpf was higher in *udu*$^{tu24}$ mutants compared with wild-type embryos in the eye and hindbrain regions (Figure 3, I–M). In summary, these results showed that *udu* mutation indeed affects cell cycle progression.

### *The Atm–Chk2 Pathway Is Activated in udu*$^{tu24}$ *Mutants Due to DNA Damage*

It has been shown that a p53 downstream target gene *p21*$^{WAF/CIP1}$, encoding a cyclin-dependent kinase inhibitor, mediates DNA damage-induced cell cycle arrest during G1/S and G2/M transition (Niculescu *et al.*, 1998). In combination with the above-described observations, we suspected that the DNA damage pathway, which functions upstream of p53, may be responsible for *udu*$^{tu24}$ phenotypes. Real-time PCR was performed to determine the expression levels of *atm*, *atr*, *chk1*, and *chk2*. It was found that *atm* and *chk2* levels are significantly up-regulated in *udu*$^{tu24}$ mutants

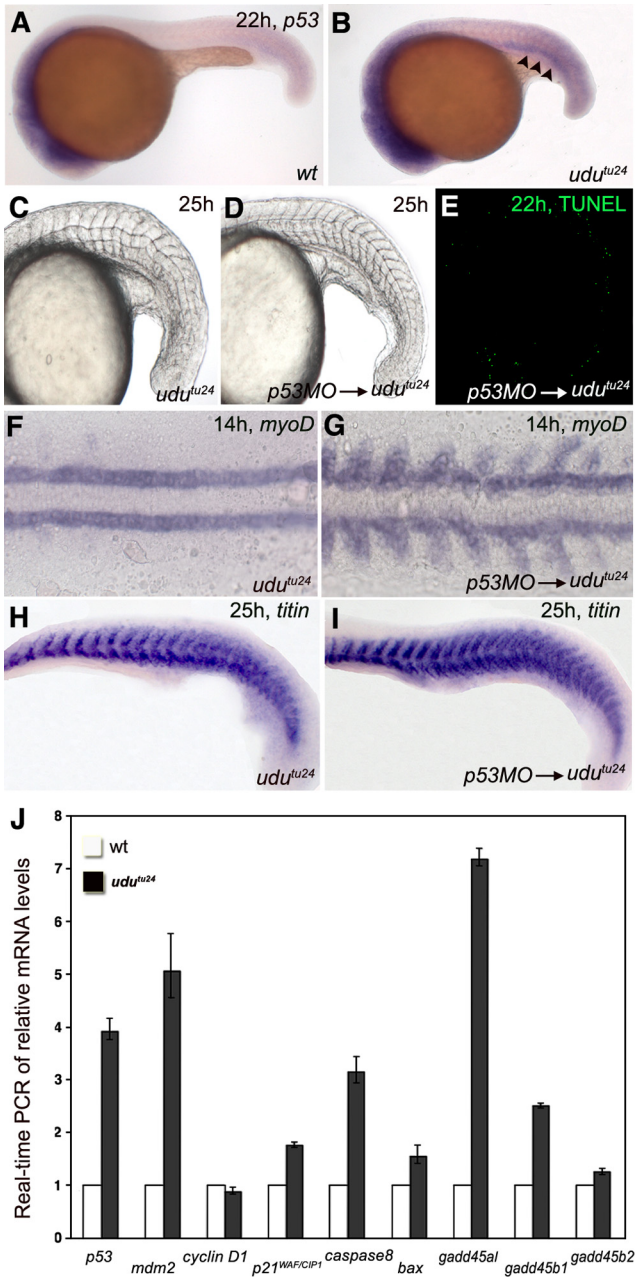


**Figure 2.** *p53* and its downstream target genes induce apoptosis in *udu*$^{tu24}$ embryos. (A and B) WISH of *p53* in the zebrafish embryos at 22 hpf displays a higher level of expression in many parts of *udu*$^{tu24}$ mutants. Arrowheads indicate pronephron. (C–E) Developmental and apoptotic defects in *udu*$^{tu24}$ embryos can be rescued by inactivating *p53* function with MO. (E) TUNEL staining of *udu*$^{tu24}$ embryos injected with 1.77 pmol of *p53*-MO. (F and G) WISH of *myoD* at 14 hpf. Note the *myoD*-striped pattern in the somites of injected embryos, whereas *myoD*-expressing cells were only found in the adaxial cells of *udu*$^{tu24}$ embryos. (H and I) Myotome boundaries of *udu*$^{tu24}$ embryos can be rescued with *p53*-MO injection as shown by *titin* at 25 hpf. (J) Real-time PCR of relative mRNA levels of 22 hpf wild-type and *udu*$^{tu24}$ embryos. *elf1a* is the endogenous control for the experiment. The histogram is depicted as average ± SD format from two independent duplicated experiments. Homozygous *udu*$^{tu24}$ embryos have elevated levels of *p53*, *mdm2*, *p21*$^{WAF/CIP1}$, *caspase 8*, *bax*, *gadd45αl*, *gadd45β1*, and *gadd45β2* and barely reduced level of *cyclin D1* compared with wild-type embryos. All embryos are showed in anterior to the left and dorsal upward.

(Figure 4A), suggesting an activation of the Atm–Chk2 pathway. Western analyses further demonstrated increased levels of Chk2 and phospho-Chk2 in *udu*$^{tu24}$ mutants (Figure 4, B and C), confirming Chk2 activation. Because Atm is activated in response to DSBs (Shiloh, 2003), we then used the neutral comet assay to analyze DSBs in dissociated cells from 22 hpf wild-type and *udu*$^{tu24}$ embryos. The resulting images resemble a "comet" with a distinct head and tail. The head is composed of intact DNA, whereas the tail consists of DSB DNA. In wild-type embryos, the fluorescence was confined to the comet head, indicating intact and undamaged DNA, whereas in *udu*$^{tu24}$ mutants, the presence of DSB DNA was depicted by the comet tail (Figure 4, D and E). Comet tail was detected in *p53*-MO-injected *udu*$^{tu24}$ mutants, in which apoptosis is inhibited, excluding the possibility that DNA defect originates from apoptosis-induced DNA fragmentation (Figure 4, F and G). Wild-type embryos subjected to UV treatment, which also causes DSB via propagation of clustered single-stranded breaks (SSBs) that occur at closely spaced DNA lesions (Jenner *et al*., 2001; Rapp and Greulich, 2004; Garinis *et al*., 2005), were used as a positive control (Figure 4H).

To elucidate whether the cellular phenotype of p53-dependent apoptosis in *udu*$^{tu24}$ mutants relies on the DNA damage checkpoint, we injected *atm*-MO and *chk2*-MO into *udu*$^{tu24}$ mutants. *atm*-MO–injected embryos showed severe developmental arrest (data not shown) as reported previously (Yamaguchi *et al*., 2008). We further tried chemical inhibitors, KU55933 and CGK733, which are kinase inhibitors of ATM and ATM/ATR, respectively (Hickson *et al*., 2004; Won *et al*., 2006). Although the somite phenotype could not be rescued, the TUNEL assay showed that treatment with KU55933 (62.5%; n = 5/8) and CGK733 (80%; n = 8/10) could significantly reduce the number of apoptotic cells (Figure 4, I–K). Moreover, posterior segmented somites were restored in 57.4% (n = 27/47) of *udu*$^{tu24}$ mutants injected with *chk2*-MO compared with uninjected *udu*$^{tu24}$ mutants at 21 hpf (Figure 4, L–N). The total number of apoptotic cells was also significantly reduced in the somite-rescued *chk2*-MO–injected *udu*$^{tu24}$ mutants (Figure 4, O–Q). These data demonstrate an activation of the Atm–Chk2–p53 signaling pathway in response to DNA damage in *udu*$^{tu24}$ mutants.

### *DNA Repair for DSB Seems Functional in udu*$^{tu24}$ *Mutants*

To dissect the mechanism that could potentially induce DNA DSB and activate the Atm–Chk2–p53 pathway, we investigated the role of Udu in cellular processes involving DNA repair and replication. Phosphorylated H2AX, referred to as γ-H2AX, can be detected within minutes after the induction of DSB and is required for the recruitment of several DNA repair proteins to the DNA damage sites (Paull *et al*., 2000). Each γ-H2AX focus is assumed to label one DSB site (Rothkamm and Löbrich, 2003). The slightly increased number of γ-H2AX foci found in non–UV-treated *udu*$^{tu24}$ mutants indicated the presence of DNA DSB, which is consistent with the previously-shown comet assay (Figure 5, A and B). After 1-h irradiation, the number of γ-H2AX foci was significantly increased, and they dispersed throughout the trunk and tail regions of both wild-type and *udu*$^{tu24}$ embryos (Figure 5, C and D). Thus, *udu*$^{tu24}$ mutants were able to response to DNA damage by recruiting DNA repair proteins via γ-H2AX. The density and intensity of γ-H2AX signals 5 h post-UV irradiation was similarly maintained in both wild-type and *udu*$^{tu24}$ embryos (Figure 5, E and F). It has been reported that repair of DNA DSBs takes a longer time compared with DNA SSBs (Rapp and Greulich, 2004). Indeed, our experimental results showed that

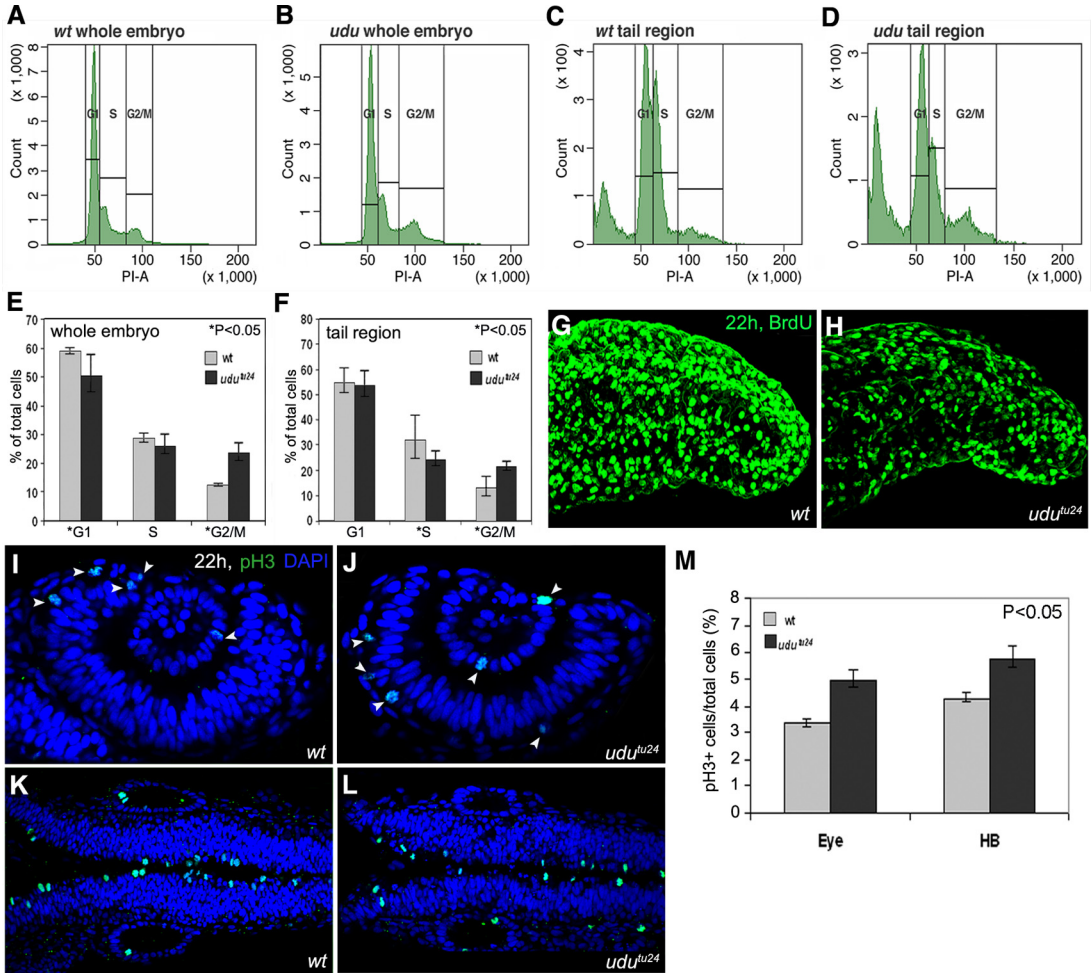


**Figure 3.** Loss of *udu* function results in aberrant cell cycle. (A–D) Representative traces from FACS analyses after PI staining of dissociated cells at 22 hpf from wild-type and $udu^{tu24}$ embryos. (A and B) Dissociated cells from whole wild-type and $udu^{tu24}$ embryos. (C and D) Dissociated cells from wild-type and $udu^{tu24}$ embryos' tail region posterior to yolk extension. (E and F) Histograms summarize experimental data from FACS analyses after PI staining of dissociated cells from (E) whole embryos and (F) tail region posterior to yolk extension. The histograms are depicted as average ± SD format from triplicate experiments. $udu^{tu24}$ embryos contain fewer cells in the G1 and S phases and have an accumulation of cells in the G2/M phase (asterisks marked those $p < 0.05$, Student's *t* test; p value for whole embryo: *G1, $p = 0.041$; S, $p = 0.151$; *G2/M, $p = 0.007$; for tail region: G1, $p = 0.05$; *S, $p = 0.035$; *G2/M, $p = 0.016$). (G and H) Projection of the lateral stacks of S phase cells labeled with BrdU at 22 hpf. Images are tail region posterior to yolk extension shown in lateral view with anterior to the left. (I–L) Wild-type and $udu^{tu24}$ embryos stained with pH3 antibody (green, arrowheads); nuclei are counterstained with DAPI (blue): eye region (I and J) and hindbrain region (K and L). (M) Percentage of pH3-positive cells in eye and hindbrain regions are obtained by counting pH3-positive cells versus total cells labeled with DAPI and are summarized in histogram, expressing in average ± SD format from four wild-type and four $udu^{tu24}$ embryos ($p < 0.05$, Student's *t* test).

cells with γ-H2AX signals were significantly reduced in the trunk and tail regions of both wild-type and $udu^{tu24}$ embryos after 24 h (data not shown) and further reduced after 31 h (Figure 5, G and H) UV irradiation. To further interrogate the effects of inhibition of apoptosis, wild-type and $udu^{tu24}$ embryos were injected with *p53*-MO. Increased γ-H2AX staining due to damaged DNA can be observed in *p53*-injected $udu^{tu24}$ embryos, because damaged cells were not cleared via apoptosis and therefore accumulated (Figure 5, I and J). Together, these results further link the loss of *udu* function with DNA damage and suggest that Udu is not essential for DSB DNA repair.

### *Udu Binds MCM Proteins and Localizes in Chromatin during DNA Replication*

To further explore the function of Udu, we engaged in the yeast two-hybrid (Y2H) screen service of Hybrigenics (Paris, France) to discover Udu-interacting partners in a cDNA library made from 18 to 20 hpf zebrafish embryos. Using PAH-L and SANT-L domains together as a bait, MCM3 and MCM4 were found to be interesting among the proteins identified from the Y2H screen. We next performed coimmunoprecipitation to examine whether both MCM3 and MCM4 really bind to PAH-L and SANT-L domains. FLAG-tagged proteins (PAH-L+SANT-L) and MYC-tagged interacting proteins (MCM3 and MCM4) were used and results demonstrated that MCM3 and MCM4 indeed bind to PAH-L and SANT-L domains of Udu (Figure 5K).

Udu protein, containing both PAH-L and SANT-L domains, has been shown to reside in the nucleus (Liu *et al.*, 2007). However, it was done in unsynchronized cells. The available Udu antibody (Liu *et al.*, 2007) failed to detect Udu in zebrafish embryos via immunohistochemical method and to gain better understanding of its function during DNA

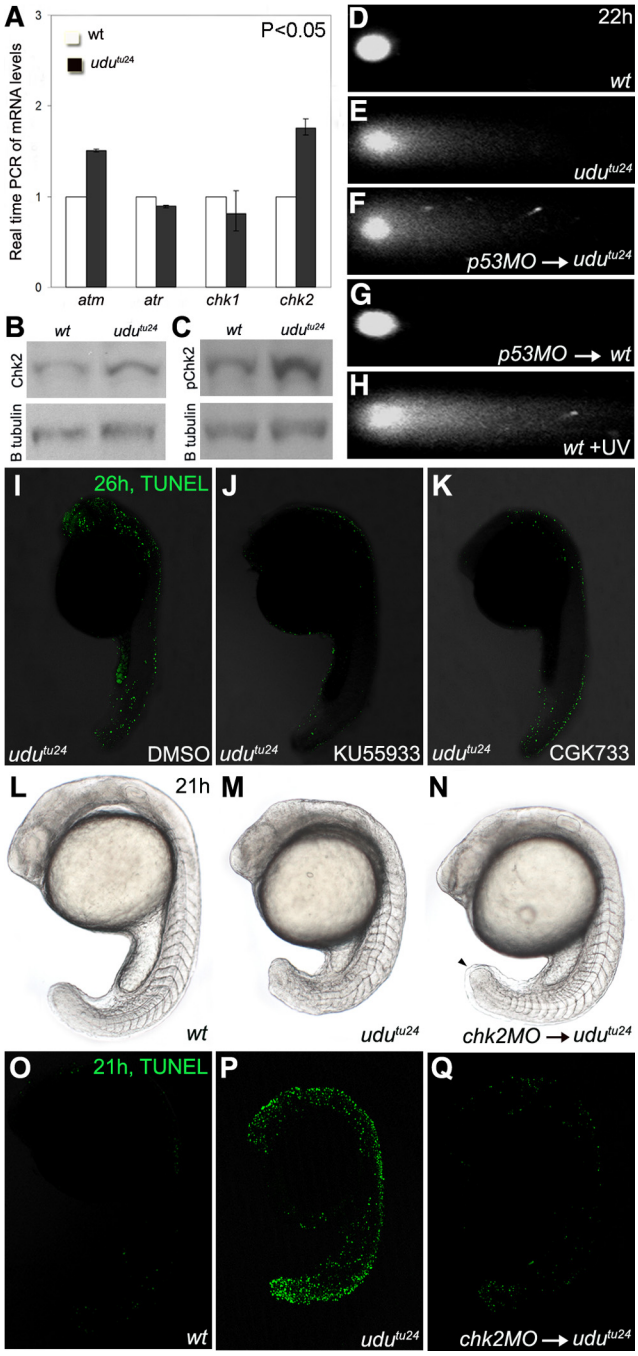


**Figure 4.** Activation of Atm-Chk2 pathway in *udu*$^{tu24}$ mutants. (A) Real-time PCR of *atm*, *atr*, *chk1* and *chk2* mRNA levels extracted from 22 hpf embryos. The histogram is depicted as average ± SD format from three independent experiments ($p < 0.05$, Student's *t* test). The transcript level of *atm* and *chk2* are significantly up-regulated in *udu*$^{tu24}$ mutants. (B and C) Western analyses showed increased levels of Chk2 and phospho-Chk2 (Ser33) in *udu*$^{tu24}$ embryos compared with wild-type embryos at 22 hpf. (D–H) Neutral single-cell electrophoresis or comet assay of untreated wild-type cells (D), untreated *udu*$^{tu24}$ cells (E), cells from *p53*-MO–injected *udu*$^{tu24}$ embryos (F), cells from *p53*-MO–injected wild-type embryos (G), and wild-type cells (H) isolated from embryos irradiated with UV for 1 h. The head is composed of intact DNA, whereas the tail consists of DNA with DSB. (I–K) TUNEL staining of *udu*$^{tu24}$ embryos treated with DMSO (I), 15 μM KU55933 (J), and 200 μM CGK733 (K) at 26 hpf. The number of TUNEL-positive cells is significantly reduced in embryos treated with KU55933 (62.5%; n = 5/8) and CGK733 (80%; n = 8/10). (L–N) Phenotypes of *chk2* morphants at 21 hpf. (N) Homozygous *udu*$^{tu24}$ embryos injected with *chk2*-MO have tail-tips that were not round-shaped but tapered (arrowhead). Somite structures are restored in 2.08 pmol *chk2*-MO–injected *udu*$^{tu24}$ embryos, compared with (M) noninjected *udu*$^{tu24}$ embryos. (O–Q) TUNEL staining of embryos at 21 hpf. (Q) The number of TUNEL-positive cells is significantly reduced in *chk2*-MO–injected *udu*$^{tu24}$ embryos, compared with (P) noninjected *udu*$^{tu24}$ embryos. (L and O) Wild-type embryos as the positive control for phenotypic observations and TUNEL assay, respectively.

replication, colocalization experiments were performed. COS7 cells were synchronized at the G1-S border with DNA polymerase inhibitor, aphidicolin (data not shown). After released from the aphidicolin block, BrdU was incorporated into the synchronized cells, fixed at different time points and coimmunostained with antibodies against BrdU and FLAG-tagged PAH-L and SANT-L. During the early S phase, BrdU incorporation was seen in granular pattern throughout the nucleus (Figure 5, L–O). Five hours after being released into S phase, cells exhibited large BrdU foci that are colocalized with PAH-L and SANT-L domains, indicating the involvement of PAH-L and SANT-L domains during DNA replication (Figure 5, P–S).

Replication of euchromatin occurs in early S phase, whereas pericentromeric heterochromatin is replicated in late S phase (Fox *et al*., 1991; O'Keefe *et al*., 1992). We further proceeded to investigate whether Udu is localized in the replicating pericentromeric heterochromatin by staining the cells for Udu or PAH-L and SANT-L domains and HP1β, a marker for pericentromeric heterochromatin (Wreggett *et al*., 1994). Indeed, Udu (and PAH-L+SANT-L) foci were colocalized with HP1β foci (Figure 5, T–W; data not shown). Together, these data suggest a possible role of Udu in protecting the genome integrity. The loss of Udu function, particularly lacking of PAH-L and SANT-L domains, can cause DNA damage, resulting in the activation of DNA damage pathway and, subsequently, cell cycle arrest and apoptosis.

## DISCUSSION

### *Udu Deficiency Activates the Atm–Chk2–p53 Signaling Pathway*

Previous studies have shown that Udu protein is critical in regulating cell cycle progression and differentiation of the primitive erythroid lineage in a p53-dependent manner in *udu*$^{sq1}$ mutants. Both *udu*$^{tu24}$ and *udu*$^{sq1}$ alleles displayed similar phenotypes and sequence analysis revealed that mutations are respectively located in exon 12 (T1461 to A) and exon 21 (T2976 to A), resulting in a premature stop codon (Liu *et al*., 2007). Although apoptosis involving in the p53 pathway has been described in *udu*$^{sq1}$ mutants, cellular events leading to an up-regulation of *p53* have not been investigated. Here, we demonstrated that *udu* apoptosis is p53-dependent and established a major role of the Atm-Chk2 signaling pathway in response to DNA damage as summarized in Figure 6.

The Mdm2 protein is a key regulator for both p53 nuclear localization and stability by actively participating in the nuclear export and degradation of p53 (Lane and Hall, 1997; Boyd *et al*., 2000; Geyer *et al*., 2000). Unexpectedly, the up-regulated *mdm2* mRNA shown in our real-time PCR is not sufficient to reverse the effects of increased p53 activation, presumably due to the increased *p53* transcript, in *udu*$^{tu24}$ mutants. Our results indicated that the Atm–Chk2 pathway

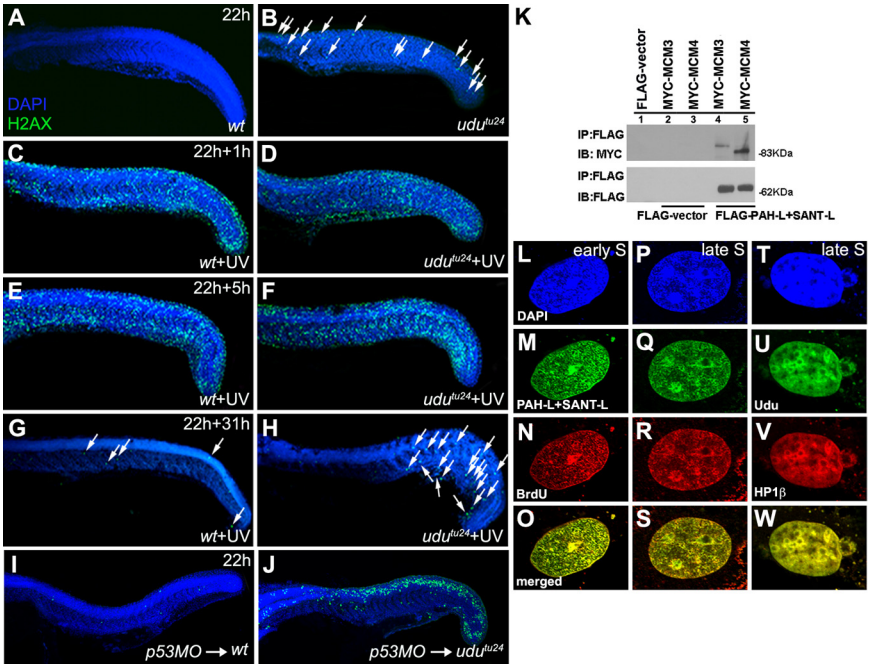


**Figure 5.** Udu dynamics and localization during DNA repair and replication. (A and B) Immunohistochemical staining of γ-H2AX in nonirradiated embryos at 22 hpf embryos: γ-H2AX foci in wild-type embryos (A) and *udu*$^{tu24}$ embryos (B). (C–H) Wild-type and *udu*$^{tu24}$ embryos were irradiated with 15 min of UV and stained with γ-H2AX at different time after irradiation. (C and D) γ-H2AX staining after 1 h post-UV treatment. Both UV-treated wild-type and *udu*$^{tu24}$ embryos showed an increased in γ-H2AX foci. Hence, in the presence of extrinsic DNA damage agents, *udu*$^{tu24}$ mutants were able to response accordingly by recruiting DNA repair proteins via the activation of γ-H2AX as indicated by the amplified fluorescence staining. (E and F) γ-H2AX staining of embryos 5 h post-UV irradiation. The level of DNA damage after 5 h of repair were similar in both wild-type and *udu*$^{tu24}$ embryos. (G and H) The number of cells with γ-H2AX signals was significantly reduced in the trunk and tail regions of wild-type and *udu*$^{tu24}$ embryos after 31 h post-UV irradiation. (I and J) γ-H2AX staining of wild-type and *udu*$^{tu24}$ embryos injected with *p53*-MO. White arrows indicate the γ-H2AX foci. (K) Coimmunoprecipitation of MYC-tagged MCM proteins and FLAG-tagged PAH-L+SANT-L domains. FLAG-tagged PAH-L+SANT-L is immunoprecipitated from the cell lysates and detected with anti-FLAG antibody as a control and with anti-MYC antibody to detect the interacting proteins, MCM3 and MCM4, shown in lanes 4 and 5. (L–O) PAH-L and SANT-L domains are associated with replication foci during S phase. COS7 cells were synchronized at the G1/S border with aphidicolin, released into S phase, labeled with BrdU and fixed at different time points and submitted to laser scanning confocal microscopy for detection: DAPI (blue) (L and P), PAH-L+SANT-L (green) (M and Q), BrdU (red) (N and R), and merged images (yellow) (O and S) show the pattern of replication in early S phase (L–O) and late S phase (P–S). (T–W) Localization of Udu in pericentromeric heterochromatin: DAPI (blue) (T), Udu (green) (U), HP1β (red) (V), and merged image (yellow) (W) shows that Udu is colocalized with HP1β, a protein marker for pericentromeric heterochromatin. IB, immunoblotting; IP, immunoprecipitation.

is activated in response to DNA damage, which thereafter causes p53-dependent apoptosis in *udu*$^{tu24}$ mutants. It has been shown that Atm phosphorylates p53 on serine-15 and Mdm2 on serine-395; Chk2 phosphorylates p53 on serine-20 (Chehab *et al.*, 1999; Maya *et al.*, 2001; Shiloh, 2001). These phosphorylation modifications prevent p53–Mdm2 association that targets p53 for proteolysis and hence may contribute to DNA damage-induced p53 stabilization (Khosravi *et al.*, 1999).

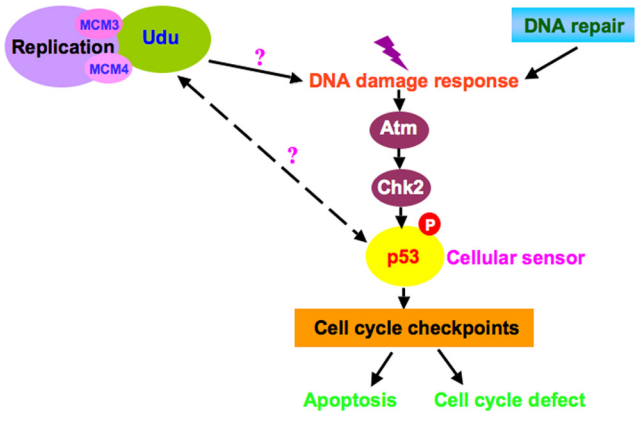


**Figure 6.** Model of Udu function in DNA damage response. Udu may be required for DNA replication by interacting with MCM3 and MCM4. Without Udu, particularly its PAH-L and SANT-L domains, replication cannot proceed properly and DNA damage response is activated via Atm-Chk2-p53 pathway. However, the molecular mechanism leading to DNA damage response is not clear. Furthermore, it is unknown whether Udu has a more direct role in regulating p53 transcriptionally. The cell cycle defects found in *udu* mutants could be replication-linked, in addition to the effect of p53.

### *Is Udu Required for DNA Replication?*

Our findings have raised the interesting question of what actually causes DNA damage in *udu*$^{tu24}$ mutants. Based on the following reasons, it is possible that DNA damage found in *udu*$^{tu24}$ mutants is caused by the dysfunction in DNA replication. First, the ability to form γ-H2AX foci after UV treatment in *udu*$^{tu24}$ mutants suggests that the DNA repair mechanism and, presumably, most of its corresponding proteins are largely unaffected. Second, Y2H and coimmunoprecipitation show that Udu binds to MCM3 and MCM4. Third, Udu localizes in chromatin during the S phase in synchronized cells. Fourth, *mcm2*, *mcm4*, and *mcm5* expression level is down-regulated in *udu*$^{sq1}$ mutants (Liu *et al.*, 2007), probably due to the elevated *p53* expression (Scian *et al.*, 2008) and/or cross-regulation between MCM proteins (Fitch *et al.*, 2003). And last, Udu contains PAH-L and SANT-L domains, which have been shown to be involved in transcription and/or chromatin remodeling.

DNA replication occurs at specialized sites, known as the replication origins, during the S phase of the cell cycle. Before DNA replication starts, the DNA helix must be unwound by MCM proteins that act as DNA helicase to allow the access of numerous accessory proteins, including DNA polymerases, proliferating cell nuclear antigen, primase, topoisomerase, and DNA ligase (Bell and Dutta, 2002). Hence, DNA replication involves dynamic changes of chromatin

structure. Studies have shown that the PAH domain is a flexible domain that could function with numerous sequence specific transcription factors and regulate gene transcription (Silverstein and Ekwall, 2005). This implies that Udu protein may form complexes with interacting partners via PAH-L repeats, together with SANT-L domain functioning as a chromatin remodeling complexes (Boyer *et al*., 2002, 2004). Our data demonstrated that PAH-L and SANT-L domains of Udu binds to MCM3 and MCM4. Hence, Udu in *udu*$^{tu24}$ mutants, which lacks both PAH-L and SANT-L domains, may be unable to interact with MCM proteins, probably leading to increased DNA damage, indicated by our comet assay. The reduction of BrdU-positive cells in *udu*$^{tu24}$ mutants further supports our notion that progression though the S phase is delayed or prevented.

MCMs proteins have been shown to be direct targets of ATM/ATR kinases (Cortez *et al*., 2004; Ishimi *et al*., 2003; Shi *et al*., 2007; Yoo *et al*., 2004), suggesting that the MCMs may be targets or effectors of the replication checkpoint. It has been shown that the phosphorylation of MCM4 in the checkpoint control inhibits DNA replication, which includes blockage of DNA fork progression through inactivation of the MCM complex (Ishimi *et al*., 2003). Thus, the DNA sequence fidelity, together with associated chromatin structure must be accurately replicated to maintain genetic and epigenetic information through cell generations. To achieve this, it is plausible that chromatin remodeling may play important roles to facilitate the many steps of replication process.

In conclusion, we provide evidence that PAH-L and SANT-L domains of Udu associates with MCM proteins and localizes in chromatin during the S phase, suggesting that these domains may be required for DNA replication. We speculate that the association of Udu with MCM proteins may provide additional factors and/or activation steps on structural modulation of MCM proteins in DNA unwinding at replication origins. Our findings warrant further study of the Udu function in DNA replication.

### *Is Udu Coupled with Cell Cycle?*

To maintain the genome stability, the cell cycle control system must ensure that replication is completed before chromosome segregation can occur. Blast searches in database revealed that the Udu protein had the highest homology to the human and mouse GON4L in both protein sequence and gene structure (Kuryshev *et al*., 2006; Liu *et al*., 2007). *Caenorhabditis elegans gon-4*, from which the name of the mammalian orthologue was derived, was identified as cell lineage regulator in gonadogenesis of *Caenorhabditis elegans*. It was also suggested that *gon-4* may control expression of genes that drive the cell cycle (Friedman *et al*., 2000). Further evidence for the involvement of GON4L in cell cycle control comes from the association of the *Drosophila* GON4L homolog, Cdp1, with cyclin D demonstrated in a Y2H screen (Zhong *et al*., 2003). Hence, these data suggest that the function of *GON4L* may be linked to cell cycle control. Actually, we also identified cell cycle defects in *udu*$^{tu24}$ mutants, although mainly through p53. It will be intriguing to revisit the phenotypes of *C. elegans gon-4* and *Drosophila cdp1* mutants and examine whether the Atm-Chk2-p53 pathway is activated and whether Udu proteins regulate cell cycle coupling with DNA replication.

In zebrafish, mutants of several proteins required for DNA replication have been identified and characterized: *mcm5* (Ryu *et al*., 2005), *DNA polymerase delta1/fla* (Plaster *et al*., 2006) and *primase/piy* (Yamaguchi *et al*., 2008). Similar to *udu* mutants, these mutants all show apoptosis, two of which are also p53-dependent and show cell cycle defects (Ryu *et al*., 2005; Plaster *et al*., 2006). Although not yet examined, retinal apoptosis in *mcm5* and *fla* mutants may depend on Atm and/or Chk2. It is unclear why *piy* mutants activate the DNA damage response via Atm-Chk2-p53 without any or little defects in DNA replication. Nevertheless, the characterization of these mutants suggests that cell cycle and DNA replication are tightly coregulated.

In summary, we have demonstrated the involvement of the Atm–Chk2–p53 pathway in causing the apoptosis in *udu*$^{tu24}$ mutants and the association of Udu with MCM proteins as well as a possible link between PAH-L and SANT-L domains and DNA replication. These findings lead us to hypothesize a possible role of Udu in maintaining or protecting the genome integrity, as the loss of *udu* function leads to an activation of the DNA damage response pathway, which potentially eliminates damaged cells via apoptosis. Overall, this could lead us to have a better understanding of Udu and its related members in the regulation of replication and the mechanism underlying p53-dependent apoptosis in maintaining stability and integrity of genome during development.

## ACKNOWLEDGMENTS

We thank Dr. Ichiro Masai for providing *chk2* MO and ATM/ATR inhibitors and members of the Jiang lab for helpful discussions. This work was supported by the Biomedical Research Council of Agency for Science, Technology and Research, Singapore.

## REFERENCES

Aasland, R., Stewart, A. F., and Gibson, T. (1996). The SANT domain: a putative DNA-binding domain in the SWI-SNF and ADA complexes, the transcriptional co-repressor N-CoR and TFIIIB. Trends Biochem. Sci. *21*, 87–88.

Abraham, R. T. (2003). Checkpoint signaling: epigenetic events sound the DNA strand-breaks alarm to the ATM protein kinase. Bioessays *25*, 627–630.

Bailis, J. M., and Forsburg, S. L. (2004). MCM proteins: DNA damage, mutagenesis and repair. Curr. Opin. Genet. Dev. *14*, 17–21.

Bell, S. P., and Dutta, A. (2002). DNA replication in eukaryotic cells. Annu. Rev. Biochem. *71*, 333–374.

Boyd, S. D., Tsai, K. Y., and Jacks, T. (2000). An intact HDM2 RING-finger domain is required for nuclear exclusion of p53. Nat. Cell Biol. *2*, 563–568.

Boyer, L. A., Langer, M. R., Crowley, K. A., Tan, S., Denu, J. M., and Peterson, C. L. (2002). Essential role for the SANT domain in the functioning of multiple chromatin remodeling enzymes. Mol. Cell *10*, 935–942.

Boyer, L. A., Latek, R. R., and Peterson, C. L. (2004). The SANT domain: a unique histone-tail-binding module? Nat. Rev. Mol. Cell Biol. *5*, 158–163.

Bunz, F., Dutriaux, A., Lengauer, C., Waldman, T., Zhou, S., Brown, J. P., Sedivy, J. M., Kinzler, K. W., and Vogelstein, B. (1998). Requirement for p53 and p21 to sustain G2 arrest after DNA damage. Science *282*, 1497–1501.

Chehab, N. H., Malikzay, A., Stavridi, E. S., and Halazonetis, T. D. (1999). Phosphorylation of Ser-20 mediates stabilization of human p53 in response to DNA damage. Proc. Natl. Acad. Sci. USA *96*, 13777–13782.

Cortez, D., Glick, G., and Elledge, S. J. (2004). Minichromosome maintenance proteins are direct targets of the ATM and ATR checkpoint kinases. Proc. Natl. Acad. Sci. USA *101*, 10078–10083.

Davuluri, G., Gong, W., Yusuff, S., Lorent, K., Muthumani, M., Dolan, A. C., and Pack, M. (2008). Mutation of the zebrafish nucleoporin *elys* sensitizes tissue progenitors to replication stress. PLoS Genet. *4*, e1000240.

Fitch, M. J., Donato, J. J., and Tye, B. K. (2003). Mcm7, a subunit of the presumptive MCM helicase, modulates its own expression in conjunction with Mcm1. J. Biol. Chem. *278*, 25408–25416.

Fornace, A. J., Jr., Jackman, J., Hollander, M. C., Hoffman-Liebermann, B., and Liebermann, D. A. (1992). Genotoxic-stress-response genes and growth-arrest genes. gadd, MyD, and other genes induced by treatments eliciting growth arrest. Ann. N.Y. Acad. Sci. *663*, 139–153.

Forsburg, S. L. (2004). Eukaryotic MCM proteins: beyond replication initiation. Microbiol. Mol. Biol. Rev. *68*, 109–131.

Fox, M. H., Arndt-Jovin, D. J., Jovin, T. M., Baumann, P. H., and Robert-Nicoud, M. (1991). Spatial and temporal distribution of DNA replication sites localized by immunofluorescence and confocal microscopy in mouse fibroblasts. J. Cell Sci. *99*, 247–253.

Friedman, L., Santa Anna-Arriola, S., Hodgkin, J., and Kimble, J. (2000). *gon-4*, a cell lineage regulator required for gonadogenesis in *Caenorhabditis elegans*. Dev. Biol. *228*, 350–362.

Fujita, M., Kiyono, T., Hayashi, Y., and Ishibashi, M. (1997). In vivo interaction of human MCM heterohexameric complexes with chromatin. Possible involvement of ATP. J. Biol. Chem. *272*, 10928–10935.

Garinis, G. A., *et al*. (2005). Transcriptome analysis reveals cyclobutane pyrimidine dimers as a major source of UV-induced DNA breaks. EMBO J. *24*, 3952–3962.

Geyer, R. K., Yu, Z. K., and Maki, C. G. (2000). The MDM2 RING-finger domain is required to promote p53 nuclear export. Nat. Cell Biol. *2*, 569–573.

Hammerschmidt, M., *et al*. (1996). Mutations affecting morphogenesis during gastrulation and tail formation in the zebrafish, *Danio rerio*. Development *123*, 143–151.

Helton, E. S., and Chen, X. (2007). p53 modulation of the DNA damage response. J. Cell. Biochem. *100*, 883–896.

Hickson, I., Zhao, Y., Richardson, C. J., Green, S. J., Martin, N. M., Orr, A. I., Reaper, P. M., Jackson, S. P., Curtin, N. J., and Smith, G. C. (2004). Identification and characterization of a novel and specific inhibitor of the ataxia-telangiectasia mutated kinase ATM. Cancer Res. *64*, 9152–9159.

Ishimi, Y., Komamura-Kohno, Y., Kwon, H. J., Yamada, K., and Nakanishi, M. (2003). Identification of MCM4 as a target of the DNA replication block checkpoint system. J. Biol. Chem. *278*, 24644–24650.

Jenner, T. J., Fulford, J., and O'Neill, P. (2001). Contribution of base lesions to radiation-induced clustered DNA damage: implication for models of radiation response. Radiat. Res. *156*, 590–593.

Jiang, Y.-J., Aerne, B. L., Smithers, L., Haddon, C., Ish-Horowicz, D., and Lewis, J. (2000). Notch signalling and the synchronization of the somite segmentation clock. Nature *408*, 475–479.

Kearsey, S. E., and Labib, K. (1998). MCM proteins: evolution, properties, and role in DNA replication. Biochim. Biophys. Acta *1398*, 113–136.

Khosravi, R., Maya, R., Gottlieb, T., Oren, M., Shiloh, Y., and Shkedy, D. (1999). Rapid ATM-dependent phosphorylation of MDM2 precedes p53 accumulation in response to DNA damage. Proc. Natl. Acad. Sci. USA *96*, 14973–14977.

Kimmel, C. B., Ballard, W. W., Kimmel, S. R., Ullmann, B., and Schilling, T. F. (1995). Stages of embryonic development of the zebrafish. Dev. Dyn. *203*, 253–310.

Kubota, Y., Mimura, S., Nishimoto, S., Masuda, T., Nojima, H., and Takisawa, H. (1997). Licensing of DNA replication by a multi-protein complex of MCM/P1 proteins in *Xenopus* eggs. EMBO J. *16*, 3320–3331.

Kuryshev, V. Y., *et al*. (2006). An anthropoid-specific segmental duplication on human chromosome 1q22. Genomics *88*, 143–151.

Labib, K., Tercero, J. A., and Diffley, J. F. (2000). Uninterrupted MCM2-7 function required for DNA replication fork progression. Science *288*, 1643–1647.

Lane, D. P. (1992). Cancer. p53, guardian of the genome. Nature *358*, 15–16.

Lane, D. P., and Hall, P. A. (1997). MDM2–arbiter of p53's destruction. Trends Biochem. Sci. *22*, 372–374.

Langheinrich, U., Hennen, E., Stott, G., and Vacun, G. (2002). Zebrafish as a model organism for the identification and characterization of drugs and genes affecting p53 signaling. Curr. Biol. *12*, 2023–2028.

Liu, Y., *et al*. (2007). The zebrafish *udu* gene encodes a novel nuclear factor and is essential for primitive erythroid cell development. Blood *110*, 99–106.

Ljungman, M. (2000). Dial 9-1-1 for p *53*, mechanisms of p53 activation by cellular stress. Neoplasia *2*, 208–225.

Mak, S. K., and Kultz, D. (2004). Gadd45 proteins induce G2/M arrest and modulate apoptosis in kidney cells exposed to hyperosmotic stress. J. Biol. Chem. *279*, 39075–39084.

Maya, R., *et al*. (2001). ATM-dependent phosphorylation of Mdm2 on serine *395*, role in p53 activation by DNA damage. Genes Dev. *15*, 1067–1077.

Melo, J. A., Cohen, J., and Toczyski, D. P. (2001). Two checkpoint complexes are independently recruited to sites of DNA damage in vivo. Genes Dev. *15*, 2809–2821.

Niculescu, A. B., 3rd, Chen, X., Smeets, M., Hengst, L., Prives, C., and Reed, S. I. (1998). Effects of p21(Cip1/Waf1) at both the G1/S and the G2/M cell cycle transitions: pRb is a critical determinant in blocking DNA replication and in preventing endoreduplication. Mol. Cell. Biol. *18*, 629–643.

O'Keefe, R. T., Henderson, S. C., and Spector, D. L. (1992). Dynamic organization of DNA replication in mammalian cell nuclei: spatially and temporally defined replication of chromosome-specific alpha-satellite DNA sequences. J. Cell Biol. *116*, 1095–1110.

Pacek, M., and Walter, J. C. (2004). A requirement for MCM7 and Cdc45 in chromosome unwinding during eukaryotic DNA replication. EMBO J. *23*, 3667–3676.

Paull, T. T., Rogakou, E. P., Yamazaki, V., Kirchgessner, C. U., Gellert, M., and Bonner, W. M. (2000). A critical role for histone H2AX in recruitment of repair factors to nuclear foci after DNA damage. Curr. Biol. *10*, 886–895.

Plaster, N., Sonntag, C., Busse, C. E., and Hammerschmidt, M. (2006). p53 deficiency rescues apoptosis and differentiation of multiple cell types in zebrafish flathead mutants deficient for zygotic DNA polymerase delta1. Cell Death Differ. *13*, 223–235.

Qiu, X., Xu, H., Haddon, C., Lewis, J., and Jiang, Y.-J. (2004). Sequence and embryonic expression of three zebrafish *fringe* genes, *lunatic fringe*, *radical fringe*, and *manic fringe*. Dev. Dyn. *231*, 621–630.

Rapp, A., and Greulich, K. O. (2004). After double-strand break induction by UV-A, homologous recombination and nonhomologous end joining cooperate at the same DSB if both systems are available. J. Cell Sci. *117*, 4935–4945.

Rothkamm, K., and Löbrich, M. (2003). Evidence for a lack of DNA double-strand break repair in human cells exposed to very low x-ray doses. Proc. Natl. Acad. Sci. USA *100*, 5057–5062.

Ryu, S., Holzschuh, J., Erhardt, S., Ettl, A. K., and Driever, W. (2005). Depletion of minichromosome maintenance protein 5 in the zebrafish retina causes cell-cycle defect and apoptosis. Proc. Natl. Acad. Sci. USA *102*, 18467–18472.

Scian, M. J., *et al*. (2008). Wild-type p53 and p73 negatively regulate expression of proliferation related genes. Oncogene *27*, 2583–2593.

Shechter, D., Ying, C. Y., and Gautier, J. (2004). DNA unwinding is an Mcm complex-dependent and ATP hydrolysis-dependent process. J. Biol. Chem. *279*, 45586–45593.

Shi, Y., Dodson, G. E., Mukhopadhyay, P. S., Shanware, N. P., Trinh, A. T., and Tibbetts, R. S. (2007). Identification of carboxyl-terminal MCM3 phosphorylation sites using polyreactive phosphospecific antibodies. J. Biol. Chem. *282*, 9236–9243.

Shieh, S. Y., Ikeda, M., Taya, Y., and Prives, C. (1997). DNA damage-induced phosphorylation of p53 alleviates inhibition by MDM2. Cell *91*, 325–334.

Shiloh, Y. (2001). ATM and ATR: networking cellular responses to DNA damage. Curr. Opin. Genet. Dev. *11*, 71–77.

Shiloh, Y. (2003). ATM and related protein kinases: safeguarding genome integrity. Nat. Rev. Cancer *3*, 155–168.

Silverstein, R. A., and Ekwall, K. (2005). Sin *3*, a flexible regulator of global gene expression and genome stability. Curr. Genet. *47*, 1–17.

Spronk, C. A., Tessari, M., Kaan, A. M., Jansen, J. F., Vermeulen, M., Stunnenberg, H. G., and Vuister, G. W. (2000). The Mad1-Sin3B interaction involves a novel helical fold. Nat. Struct. Biol. *7*, 1100–1104.

Tye, B. K. (1999). MCM proteins in DNA replication. Annu. Rev. Biochem. *68*, 649–686.

Vairapandi, M., Balliet, A. G., Fornace, A. J., Jr., Hoffman, B., and Liebermann, D. A. (1996). The differentiation primary response gene MyD118, related to GADD45, encodes for a nuclear protein which interacts with PCNA and p21WAF1/CIP1. Oncogene *12*, 2579–2594.

Waldman, T., Kinzler, K. W., and Vogelstein, B. (1995). p21 is necessary for the p53-mediated G1 arrest in human cancer cells. Cancer Res. *55*, 5187–5190.

Wang, H., Clark, I., Nicholson, P. R., Herskowitz, I., and Stillman, D. J. (1990). The *Saccharomyces cerevisiae* SIN3 gene, a negative regulator of HO, contains four paired amphipathic helix motifs. Mol. Cell. Biol. *10*, 5927–5936.

Wang, X. W., Zhan, Q., Coursen, J. D., Khan, M. A., Kontny, H. U., Yu, L., Hollander, M. C., O'Connor, P. M., Fornace, A. J., Jr., and Harris, C. C. (1999). GADD45 induction of a G2/M cell cycle checkpoint. Proc. Natl. Acad. Sci. USA *96*, 3706–3711.

Weinberg, E. S., Allende, M. L., Kelly, C. S., Abdelhamid, A., Murakami, T., Andermann, P., Doerre, O. G., Grunwald, D. J., and Riggleman, B. (1996).

Developmental regulation of zebrafish *MyoD* in wild-type, no tail and spadetail embryos. Development *122*, 271–280.

Won, J., Kim, M., Kim, N., Ahn, J. H., Lee, W. G., Kim, S. S., Chang, K. Y., Yi, Y. W., and Kim, T. K. (2006). Small molecule-based reversible reprogramming of cellular lifespan. Nat. Chem. Biol. *2*, 369–374.

Wreggett, K. A., Hill, F., James, P. S., Hutchings, A., Butcher, G. W., and Singh, P. B. (1994). A mammalian homologue of *Drosophila* heterochromatin protein 1 (HP1) is a component of constitutive heterochromatin. Cytogenet. Cell. Genet. *66*, 99–103.

Yamaguchi, M., Fujimori-Tonou, N., Yoshimura, Y., Kishi, T., Okamoto, H., and Masai, I. (2008). Mutation of DNA primase causes extensive apoptosis of retinal neurons through the activation of DNA damage checkpoint and tumor suppressor p53. Development *135*, 1247–1257.

Yamamoto, A., Amacher, S. L., Kim, S.-H., Geissert, D., Kimmel, C. B., and De Robertis, E. M. (1998). Zebrafish *paraxial protocadherin* is a downstream target of *spadetail* involved in morphogenesis of gastrula mesoderm. Development *125*, 3389–3397.

Yoo, H. Y., Shevchenko, A., Shevchenko, A., and Dunphy, W. G. (2004). Mcm2 is a direct substrate of ATM and ATR during DNA damage and DNA replication checkpoint responses. J. Biol. Chem. *279*, 53353–53364.

Zhong, J., Zhang, H., Stanyon, C. A., Tromp, G., and Finley, R. L., Jr. (2003). A strategy for constructing large protein interaction maps using the yeast two-hybrid system: regulated expression arrays and two-phase mating. Genome Res. *13*, 2691–2699.

Zhou, B. B., and Elledge, S. J. (2000). The DNA damage response: putting checkpoints in perspective. Nature *408*, 433–439.